ELSEVIER

Journal of Materials Processing Technology 82 (1998) 61–77

Journal of Materials Processing Technology

An analytical evaluation of the cutting forces in orthogonal cutting using a dynamic model of the shear zone with parallel boundaries

M.T. Hayajneh, V.P. Astakhov *, M.O.M. Osman

Deep-Hole Machining Centre, Mechanical Engineering Department, Concordia University, 1455 de Maisonneuve Blvd. WEst, Montreal, Quebec H3G 1M8, Canada

Received 2 April 1997

Abstract

A shear zone model with parallel boundaries is used to evaluate the dynamic cutting forces in orthogonal cutting. The cutting system was modeled using a single degree-of-freedom dynamic system where the variations of the cutting forces are represented by their total differentials. The influence of temperature on the flow shear stress of workpiece material is accounted for. The experimental verification of the proposed model was performed using a two-component piezoelectric dynamometer and adopting the rotating cutting tool–stationary workpiece procedure. The dynamometer was calibrated for static and dynamic outputs and techniques were employed for increasing the measurement accuracy and reducing cross-influence by obtaining the elements of transfer and coherent functions. Experiments were carried out to measure the dynamic fluctuations of the force components. The experimental results show good agreement with the theoretical evaluations of the cutting force components.

Keywords: Metal cutting; Dynamic modelling; Cutting forces

1. Introduction

A metal cutting system essentially comprises the cutting process and the tool layout. The cutting process involves the removal of metal in the form of chips from the workpiece by the action of the cutting tool, which latter is coupled to the machine structure through different elastic elements. Thus, the tool traces a uniform path relative to the workpiece. Normally, any small vibration caused by occasional disturbances, such as inhomogeneity of the work material and the run-out and misalignment of the workpiece, would be damped out by the structure of the cutting system. Sometimes, however, the disturbances are maintained and the system becomes unstable, such that the relative periodic displacement between the tool and the workpiece may build up to a large amplitude. This relative periodic motion between the cutting tool and the workpiece is known as chatter [1].

Chatter imposes an undesirable limit on machine tool performance because it can impede the maintaining of the work-surface finish and also it can have an adverse effect on the part dimensional accuracy and the cutting tool life.

In order to study chatter, it is important to distinguish the sources of vibrations. Basically, machining vibrations are usually classified into the following four main categories [1]:

1. Free vibration which may be initiated by some impact or shock. This vibration usually decays under the damping action of the machine tool.
2. Forced vibration caused by a source other than cutting. This may be initiated by unbalance in the machine-tool drive. Knowing the source of these forced vibrations, they can be prevented by redesign of the machine tool structure.

* Corresponding author. Tel.: +1 514 8488671; fax: +1 514 8483175; e-mail: astvik@vax2.concordia.ca

0924-0136/98/$19.00
PII S0924-0136(98)00021-1

3. Forced vibration initiated by the inherent periodicity in the cutting process, such as the built-up edge and discontinuity of the chip.
4. Self-excited vibration. This type is classified into regenerative and a non-regenerative chatter. Regenerative effect is caused by the superposition of successive cuts, where the tool removes a wavy surface generated in the previous pass. Non-regenerative vibration is maintained by cutting force fluctuations that are induced by cutting tool–workpiece relative displacement of periodic nature.

In order to understand the mechanisms leading to chatter, it is essential to know how the cutting forces vary with variation of the cutting conditions and of the tool–workpiece relative motion. The cutting forces depend on a large number of cutting system parameters, which make the formulation of an analytical dynamic cutting force model a rather difficult task. Many techniques have been developed over the past 50 years for machine tool-cutting process identification. The general approach of these techniques is to assume that the cutting forces are an approximately linear function of the relative tool–workpiece position and velocity [3]. The coefficients of this function, known as dynamic force coefficients, are the induced stiffness and the damping. Traditionally, the dynamic force functions are assumed to be linear expressions in terms of a number of time-dependent variables, which include the inner and outer modulations of the uncut chip thickness and their first time derivatives. The coefficients of these variation terms may be determined through an experimental or an analytical technique. The experimental technique is to develop an experimental method for direct measurement of the transfer function between the cutting force and the variables in the modulation of the uncut chip thickness [3–5]. The experimental method is highly empirical and requires very sophisticated test apparatus and analysis procedures.

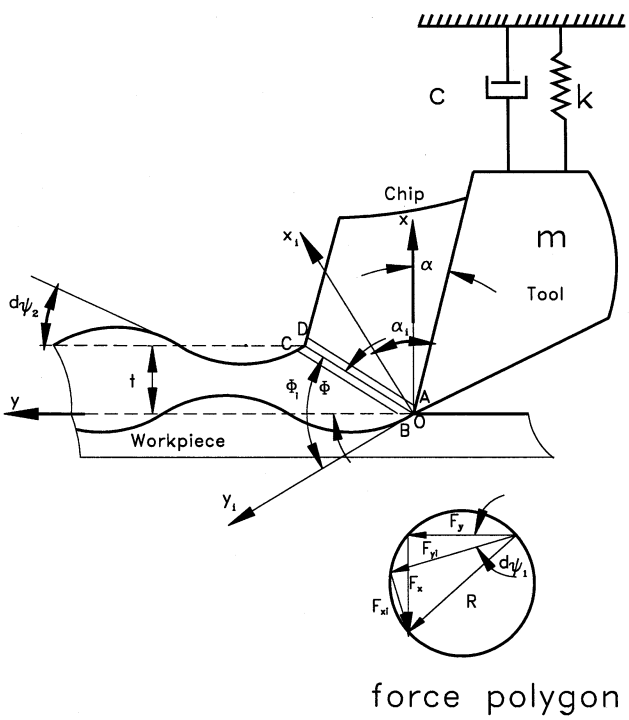

Fig. 1. A model of a shear zone with parallel boundaries as applied to evaluate the dynamic cutting forces.

Table 1
Cutting conditions for the simulation study

Workpiece material	Hot finished mild steel 0.25% C
Cutting tool	Carbide inserts (rake angles 0, 5, 10°)
Width of cut	3.5 mm
Work surface	Sinusoidal wave form of 0.05 mm amplitude
Tool vibration	Sinusoidal wave form of 0.05 mm amplitude
Cutting method	Orthogonal dry cutting
Clearance angle	10°

The promising way to formulate a proper dynamic cutting force is in using the mechanics of chip formation [2,6,7]. However, the models for chip formation used so far for this purpose are not in good agreement with the results of experiments. For example, Wu and Liu [8,9] and Wu [10–12] developed a dynamic cutting force model the single shear plane model for orthogonal cutting, which model is known for its shortcomings [13,14]. Therefore, it is reasonable to suggest that a new model of chip formation that is in better agreements with experimental result should be used.

Astakhov and Osman [13] proposed a model of chip formation with parallel boundaries which appears to be free from many of the known contradictions associated with the other known models. It would appear to be logical to incorporate it into the dynamic analysis of the cutting forces. This is the main objective of the present work.

2. Dynamic model of shear zone with parallel boundaries

2.1. General force model

Since the dynamic cutting process is very complex, the real machining system is approximated by a single-degree-of-freedom dynamic system, shown in Fig. 1. In this figure, a flexible cutting tool, vibrating normal to the cutting direction, is set to remove a layer of work material with a wavy top surface produced during previous cuts. The cutting speed, the mean uncut chip thickness, and the rake angle are preset to be v, t, and α, respectively. The coordinate system, illustrated in Fig. 1, is described as follows: (i) the x-axis is normal to the direction of the cutting speed and this axis will be referred as the vibration axis; (ii) the y-axis is perpendicular to the x-axis as shown in Fig. 1.

At any instant, the tool tip has a displacement x_1 along the vibration axis, whilst the surface end of the shear plane has a displacement x_2 relative to its equilibrium position, as shown in Fig. 1. The oscillation velocities of the tool tip and the surface end of the shear plane are denoted by $\dot{x}_1$ and $\dot{x}_2$, respectively.

It is known [15] that for steady-state machining the cutting forces are determined only by an invariable cutting configuration. Once that configuration is known, the cutting force components acting along the corresponding axes, namely the tangential F_y and the radial F_x cutting force (Fig. 1) can be determined as follows:

$$F_y = \frac{F_s \cos\alpha + F_f \sin\phi}{\cos(\phi - \alpha)}$$

$$F_x = \frac{F_f \cos\phi - F_s \sin\alpha}{\cos(\phi - \alpha)} \quad (1)$$

where F_s is the shear force along the shear zone boundaries, F_f is the tangential force on the rake face and ϕ is the shear angle.

Since in the present study the configuration of the cutting system is considered to be variable then the dynamic values of these forces should be considered as functions of the corresponding dynamic cutting parameters such as shear force, shear angle, and rake angle, which are denoted as F_{fi}, F_{si}, ϕ_i, and α_i, respectively. Therefore, a general force model may be represented in the following form:

$$F_{yi} = \frac{F_{si} \cos\alpha_i + F_{fi} \sin\phi_i}{\cos(\phi_i - \alpha_i)}$$

$$F_{xi} = \frac{F_{fi} \cos\phi_i - F_{si} \sin\alpha_i}{\cos(\phi_i - \alpha_i)} \quad (2)$$

The dynamic value of each model's component may be thought of as the sum of its steady-state value and its incremental variation as follows:

$$F_{yi} = F_y + \mathrm{d}F_y$$

$$F_{xi} = F_x + \mathrm{d}F_x$$

$$F_{si} = F_s + \mathrm{d}F_s$$

$$F_{fi} = F_f + \mathrm{d}F_f$$

$$\alpha_i = \alpha + \mathrm{d}\alpha$$

$$\phi_i = \phi + \mathrm{d}\phi \quad (3)$$

Table 2
Cutting parameters for the simulation study

	Series 1	Series 2	Series 3	Series 4
Objective: effect of	Feed	Speed	Rake angle	Frequency
Feed (mm rev^{-1})	0.075–0.300	0.19	0.19	0.19
Speed (m min^{-1})	140	60–240	140	140
Rake angle (deg)	5	5	0–10	5
Frequency (Hz)	120	120	120	60–300

2.2. Determination of the cutting force components

The incremental variations of the cutting forces F_y and F_x may be represented by their total differentials. Using Eq. (2) and neglecting the terms of high orders, one may obtain these incremental variations in the following form:

$$\mathrm{d}F_y = g_1\,\mathrm{d}F_s + g_2\,\mathrm{d}F_f + g_3\,\mathrm{d}\phi + g_4\,\mathrm{d}\alpha$$

$$\mathrm{d}F_x = e_1\,\mathrm{d}F_s + e_2\,\mathrm{d}F_f + e_3\,\mathrm{d}\phi + e_4\,\mathrm{d}\alpha \quad (4)$$

where the coefficients of Eq. (4) are:

$$g_1 = \frac{\cos\alpha}{\cos(\phi - \alpha)}$$

$$g_2 = \frac{\sin\phi}{\cos(\phi - \alpha)}$$

$$g_3 = \frac{F_f \cos\phi \cos(\phi - \alpha) + (F_s \cos\alpha + F_f \sin\phi)\sin(\phi - \alpha)}{\cos^2(\phi - \alpha)}$$

$$g_4 = \frac{-F_s \sin\alpha \cos(\phi - \alpha) + (F_s \cos\alpha + F_f \sin\phi)\sin(\phi - \alpha)}{\alpha)\cos^2(\phi - \alpha)} \quad (5)$$

and:

$$e_1 = -\frac{\sin\alpha}{\cos(\phi - \alpha)}$$

$$e_2 = \frac{\cos\phi}{\cos(\phi - \alpha)}$$

$$e_3 = \frac{-F_f \sin\phi \cos(\phi - \alpha) + (F_f \cos\phi - F_s \sin\alpha)\sin(\phi - \alpha)\cos^2(\phi - \alpha)}{}$$

$$e_4 = \frac{-F_s \cos\alpha \cos(\phi - \alpha) + (F_f \cos\phi - F_s \sin\alpha)\sin(\phi - \alpha)\cos^2(\phi - \alpha)}{} \quad (6)$$

It is known [15] that the shearing force F_s is calculated as:

$$F_s = k\frac{tb}{\sin\phi} \quad (7)$$

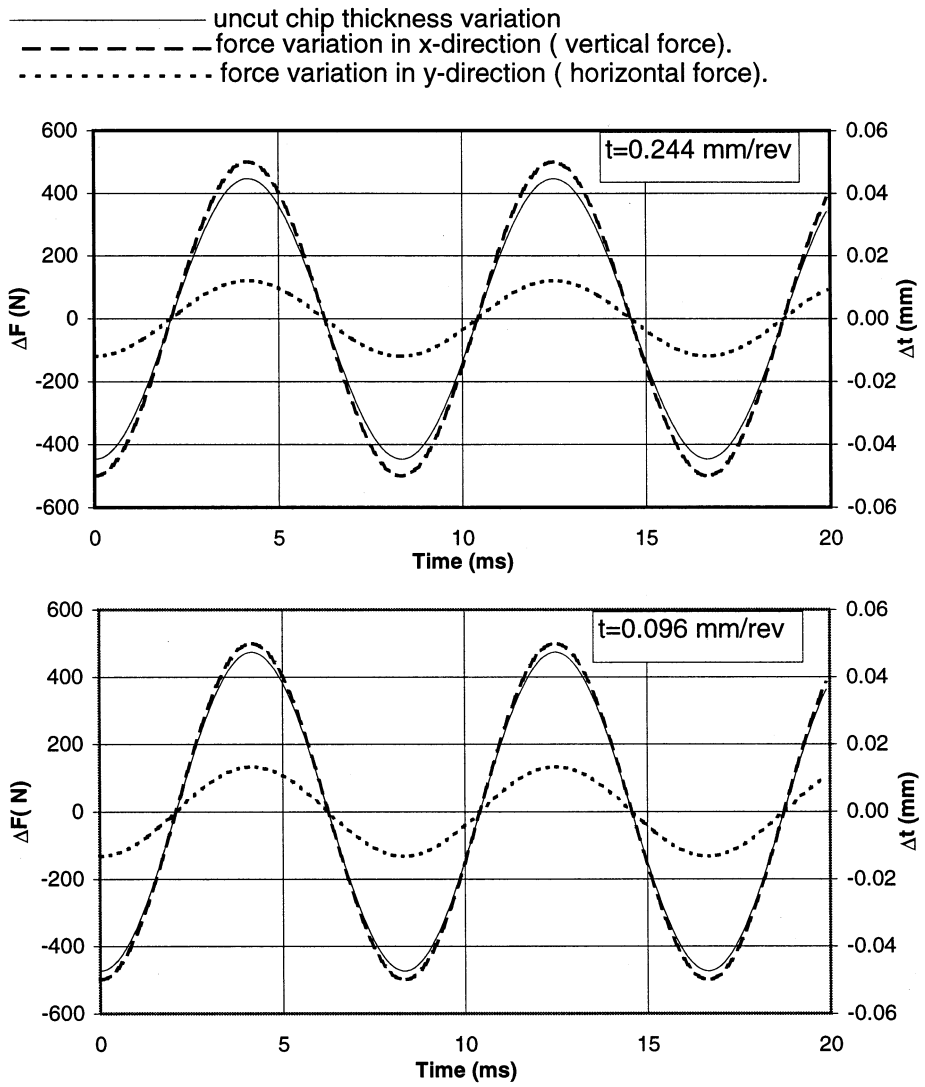

Fig. 2. Simulation results (Series 1): $v = 140$ m min^{-1}, $\alpha = 5°$, frequency = 120 Hz, $b = 3.5$ mm.

where k is the flow shear stress in the shear zone; b is the width of cut; t is the uncut chip thickness; and ϕ is the shear angle.

It is also known that the flow shear stress of the workpiece material is temperature dependent and decreases at a constant rate with temperature [16]. It has been shown by Kushner [17] that for a vast variety of steels, the flow shear stress may be related to the ultimate strength and temperature as follows:

$$k = \sigma_{ult}(1 - 0.0005T) \tag{8}$$

where k is the flow shear stress of the workpiece material (MPa); σ_{ult} is ultimate tensile strength of the workpiece material (MPa) at 20°C, and T is the temperature in the shear zone (°C).

Oxley [14] proposed to calculate the temperature in the shear zone as:

$$T_s = \frac{\sigma_{ult}}{c_v} \tag{9}$$

where c_v is the specific heat capacity at constant volume of deformed material and is the final shear strain which is known [15] to be:

$$\gamma = \frac{\cos\alpha}{\sin\phi\,\cos(\phi - \alpha)} \tag{10}$$

Substituting Eqs. (8)–(10) into Eq. (7), one can obtain:

$$F_s = \sigma_{ult} tb\left(1 - 0.0005\,\frac{\sigma_{ult}\dfrac{\cos\alpha}{\sin\phi\,\cos(\phi-\alpha)}}{c_v}\right)\frac{1}{\sin\phi} \tag{11}$$

The incremental variation of the shearing force F_s may be represented by its total differential. Using Eq. (11) and neglecting the terms of high orders, one may obtain:

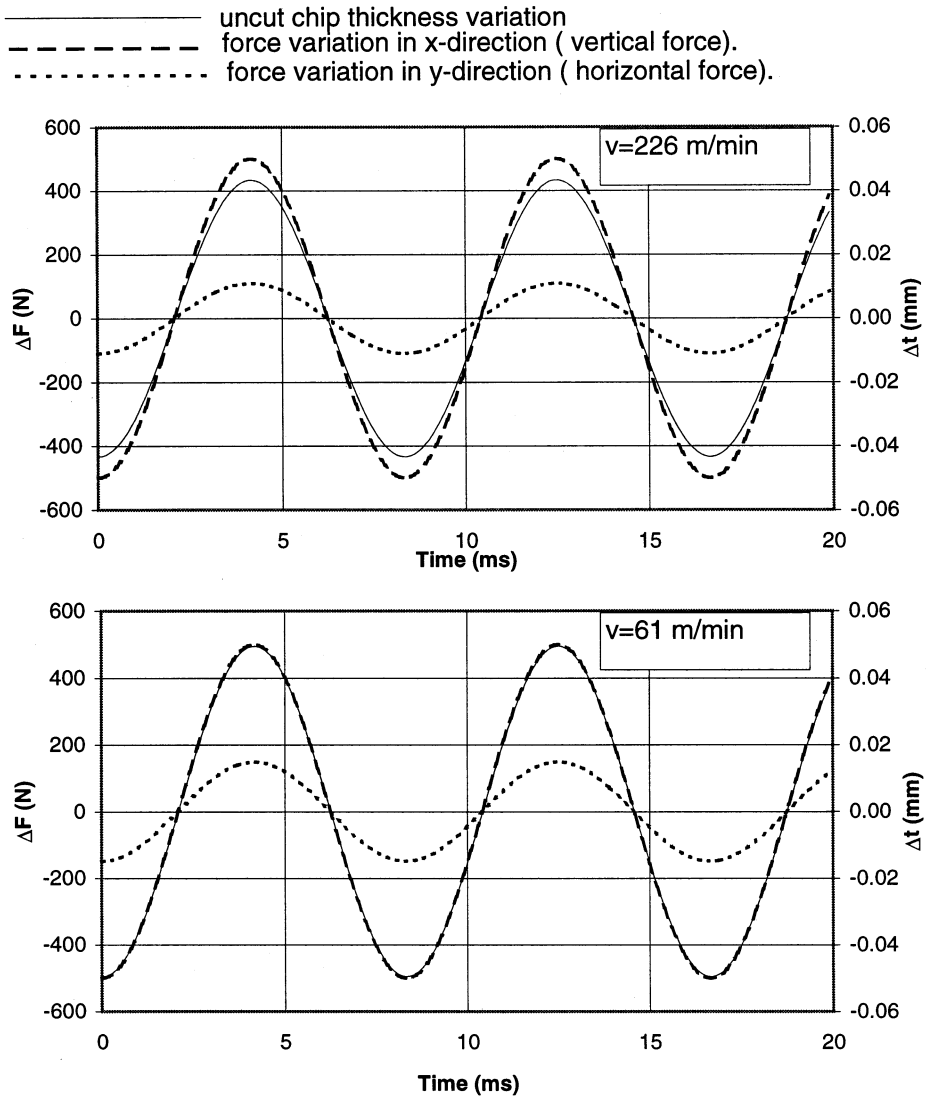

Fig. 3. Simulation results (Series 2): $t = 0.19$ mm rev^{-1}, $\alpha = 5°$, frequency = 120 Hz, $b = 3.5$ mm.

$$dF_s = n_1\,dt + n_2\,d\phi + n_3\,d\alpha \tag{12}$$

where the coefficients n_1, n_2 and n_3 are calculated as:

$$n_1 = \sigma_{ult} b \left[\frac{1}{\sin\phi} - 0.0005 \frac{\sigma_{ult}}{c_v} \frac{\cos\alpha}{\sin^2\phi\cos(\phi-\alpha)} \right]$$

$$n_2 = \sigma_{ult} t b \left[-\frac{\cos\phi}{\sin^2\phi} + 0.0005 \frac{\sigma_{ult}}{c_v} \frac{\cos\alpha(-\sin^2\phi\sin(\phi-\alpha) + 2\sin\phi\cos\phi\cos(\phi-\alpha))}{\sin^4\phi\cos^2(\phi-\alpha)} \right]$$

$$n_3 = \sigma_{ult} t b \left[0.0005 \frac{\sigma_{ult}}{c_v} \frac{\sin^2\phi\cos(\phi-\alpha)\sin\alpha - \cos\alpha\sin^2\phi\sin(\phi-\alpha)}{\sin^4\phi\cos^2(\phi-\alpha)} \right] \tag{13}$$

The tangential force F_f acting along the tool–chip interface can be obtained as [18]:

$$F_f = k_1 b l_{ef} \tag{14}$$

Here, l_{ef} is the effective length of the tool–chip interface and k_1 is the flow shear stress along the chip–tool interface, which latter can be obtained from the thermomechanical model knowing the tool–chip interface temperature.

The shear flow stress in the tool–chip interface can be calculated using the results of the study of the model of chip formation with parallel boundaries [13] as follows:

$$F_f = \sigma_{ult} b l_{ef} \left[1 - 0.00395 \left(\frac{\sigma_{ult}}{100 c_v} - 0.0005 \frac{\sigma_{ult}^2}{100 c_v^2} \times \frac{\cos\sigma}{\sin\phi\cos(\phi-\alpha)} \right)^{0.8} \left(\frac{l_{st} v}{\zeta w} \right)^{0.4} \right] \tag{15}$$

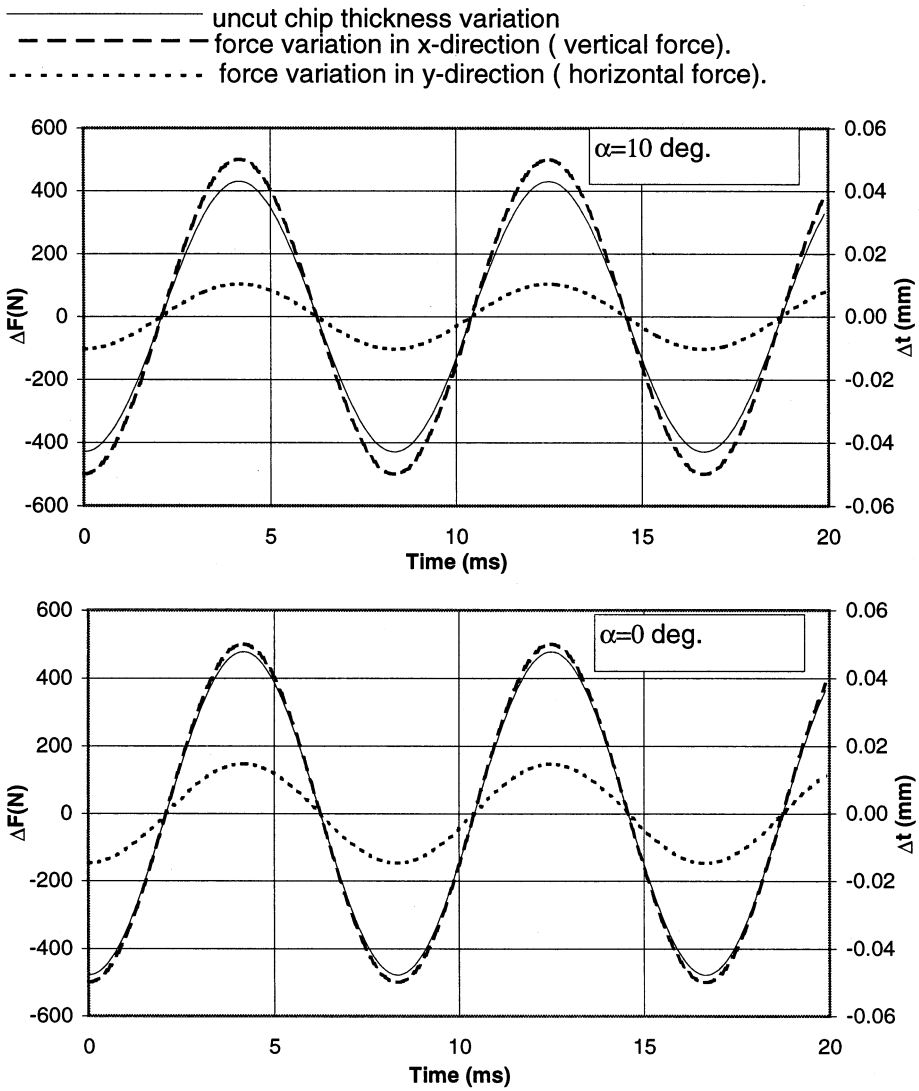

Fig. 4. Simulation results (Series 3): $v = 140$ m min^{-1}, $t = 0.19$ mm rev^{-1}, frequency = 120 Hz, $b = 3.5$ mm.

Here, l_{st} is the length of the plastic part of the tool–chip interface; w is the thermal diffuseness of workpiece material; and ζ is the chip compression ratio.

Tangential force F_f along the tool–chip interface can be obtained by substituting Eq. (15) into Eq. (14) as:

$$F_f = \sigma_{ult} b l_{ef} \left[1 - 0.00395 \times \left(\frac{\sigma_{ult}}{100 c_v} - 0.0005 \frac{\sigma_{ult}^2}{100 c_v^2} \frac{\cos\alpha}{\sin\phi \cos(\phi - \alpha)} \right)^{0.8} \left(\frac{l_{st} v}{\zeta w} \right)^{0.4} \right] \quad (16)$$

It is also known [18] that the full tool–chip interface length l_f, the effective length l_{ef} and the length of the plastic part of the tool–chip interface l_{st} can be represented in terms of chip compression ratio ζ as follow:

$$l_f = t\zeta^{1.5}$$

$$l_{ef} = \frac{2}{3} l_f = \frac{2}{3} t\zeta^{1.5}$$

$$l_{st} = \frac{3}{4} l_{ef} = \frac{3}{4}\frac{2}{3} l_f = \frac{1}{2} t\zeta^{1.5} \quad (17)$$

Substituting Eq. (17) into Eq. (16) and rearranging terms, one can obtain:

$$F_f = C_1 \left[t\zeta^{1.5} - C_2 \left(C_3 - C_4 \frac{\cos\alpha}{\sin\phi \cos(\phi - \alpha)} \right)^{0.8} \times \left(\frac{t^{3.5} \zeta^{4.25} v}{2w} \right) 0.4 \right] \quad (18)$$

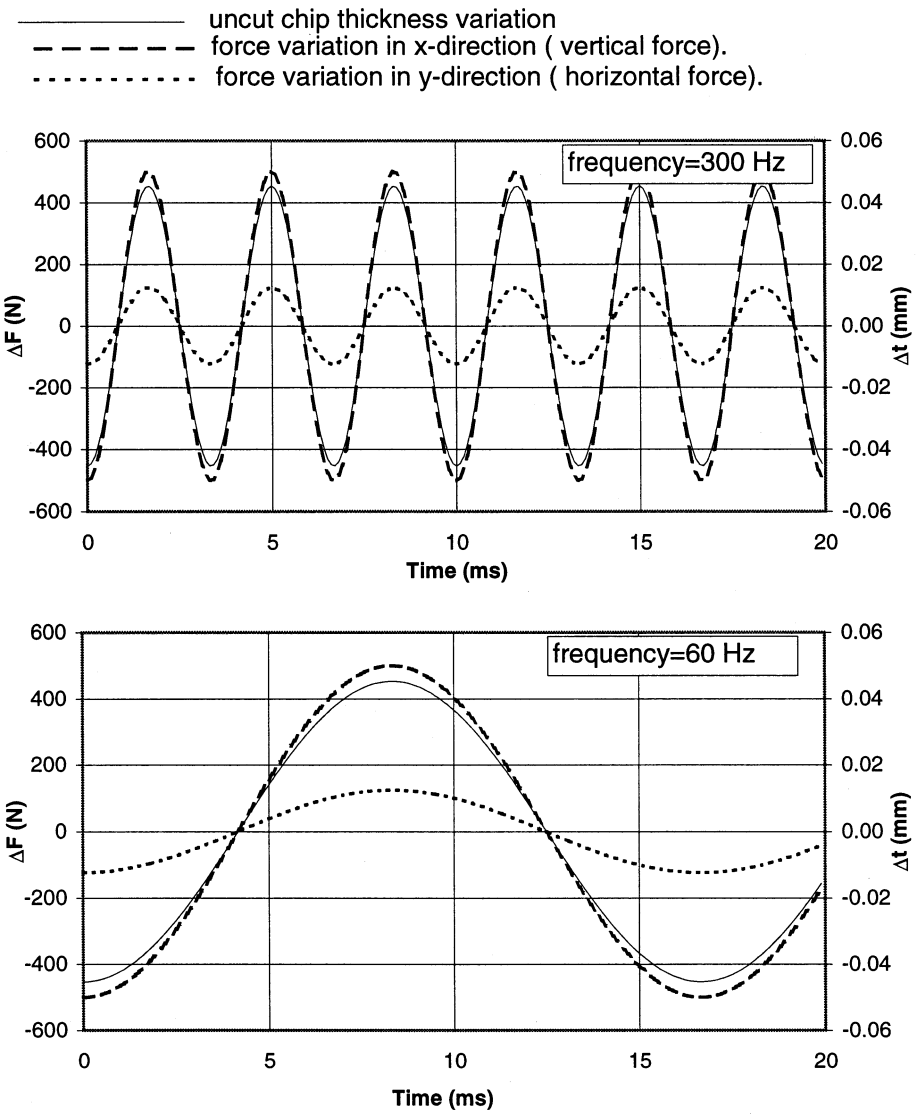

Fig. 5. Simulation results (Series 4): $v = 140$ m min^{-1}, $t = 0.19$ mm rev^{-1}, $\alpha = 5°$, $b = 3.5$ mm.

where:

$$C_1 = \frac{2}{3}\sigma_{ult} b; \qquad C_2 = 0.00395; \qquad C_3 = \frac{\sigma_{ult}}{100 c_v};$$

$$C_4 = 0.0005\frac{\sigma_{ult}^2}{100 c_v^2} \tag{19}$$

The incremental variation of the shearing force may be represented by its total differential. Using Eq. (18) and neglecting the terms of high orders, one may obtain:

$$dF_f = m_1\, dt + m_2\, d\zeta + m_3\, dv + m_4\, d\phi + m_5\, d\alpha \tag{20}$$

where m_1, m_2, m_3, m_4 and m_5 are:

$$m_1 = C_1\left[\zeta^{1.5} - 1.4C_2\frac{t^{2.5}\zeta^{4.25}v}{2w} \times \left(C_3 - C_4\frac{\cos\alpha}{\sin\phi\cos(\phi-\alpha)}\right)^{0.8}\left(\frac{t^{3.5}\zeta^{4.25}v}{2w}\right)^{-0.6}\right]$$

$$m_2 = C_1\left[1.5t\zeta^{0.5} - C_2{*}\frac{17}{10}\frac{t^{3.5}\zeta^{3.25}v}{2w}\left(C_3 - C_4\frac{\cos\alpha}{\sin\phi\cos(\phi-\alpha)}\right)^{0.8} \times \left(\frac{t^{3.5}\zeta^{4.25}v}{2w}\right)^{-0.6}\right]$$

$$m_3 = C_1\left[-C_2\frac{t^{3.5}\zeta^{4.25}}{2w}\left(C_3 - C_4\frac{\cos\alpha}{\sin\phi\cos(\phi-\alpha)}\right)^{0.8} \times \left(\frac{t^{3.5}\zeta^{4.25}v}{2w}\right)^{-0.6}\right]$$

$$m_4 = C_1\left[-0.8C_2C_4\frac{\cos\alpha\cos(2\phi-\alpha)}{\sin^2\phi\cos^2(\phi-\alpha)} \times \left(C_3 - C_4\frac{\cos\alpha}{\sin\phi\cos(\phi-\alpha)}\right)^{-0.2}\left(\frac{t^{3.5}\zeta^{4.25}v}{2w}\right)^{0.4}\right]$$

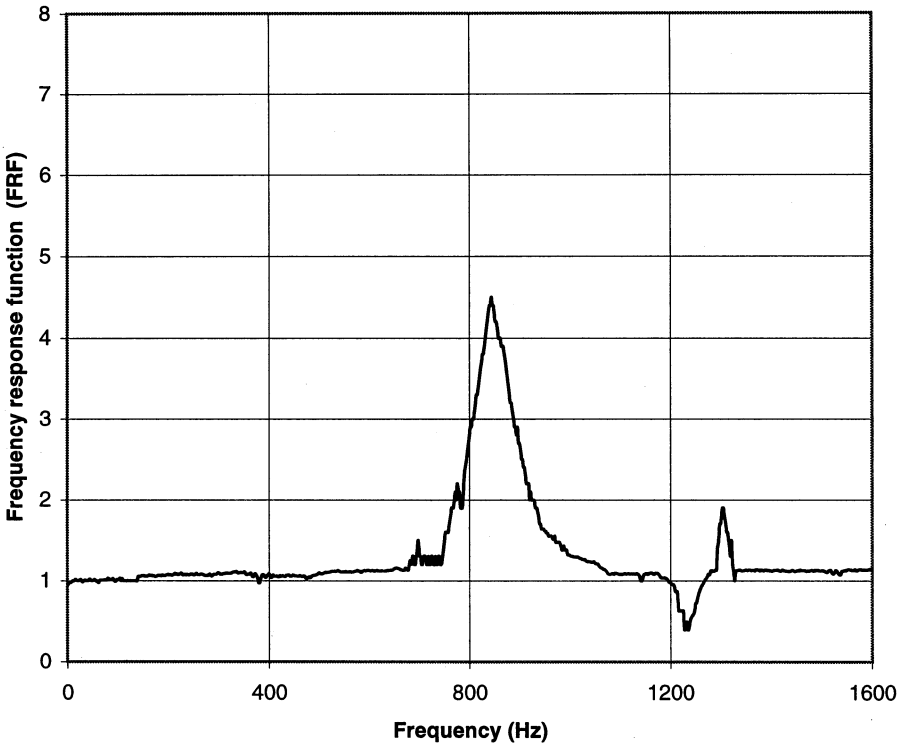

Fig. 6. Frequency response function of the thrust force signal vs. the hammer signal.

$$m_5 = C_1 \left[0.8 C_2 C_4 \frac{\sin(\phi - 2\alpha)}{\sin\phi \cos^2(\phi - \alpha)} \times \left(C_3 - C_4 \frac{\cos\alpha}{\sin\phi \cos(\phi - \alpha)} \right)^{-0.2} \left(\frac{t^{3.5} \zeta^{4.25} v}{2w} \right)^{0.4} \right] \quad (21)$$

2.3. Influence of incremental variations of the shear angle

The model of shear zone with parallel boundaries utilizes Merchant's expression for the shear angle [15]:

$$\phi = \tan^{-1} \left(\frac{\cos\alpha}{\zeta - \sin\alpha} \right) \quad (22)$$

Here, the chip compression ratio and the rake angle are constant. However, this is not the case in the present consideration. Therefore, dynamic variations of these parameters should be considered.

The incremental variation of the shear angle may be represented by its total differential in the following form:

$$\mathrm{d}\phi = \frac{\partial\phi}{\mathrm{d}\zeta} \mathrm{d}\zeta + \frac{\partial\phi}{\partial\alpha} \mathrm{d}\alpha + \frac{\partial\phi}{\partial\alpha} \mathrm{d}\psi \quad (23)$$

As can be seen, Eq. (23) contains three terms instead of two as might be expected from Eq. (22). This may be explained as follows. The angle ψ represent the angle between the free surface of the workpiece and the y-direction. Since in the steady-state consideration this angle is zero, it does not appear in Eq. (22). In the dynamic consideration, however, this angle plays an important role. In wave cutting, the dynamic direction of cutting is at an angle $\mathrm{d}\psi_1$ to the direction against which the rake angle of the tool is measured, which increases the rake angle. In wave removing, the opposite is the case so that $\mathrm{d}\psi_2$ decreases the rake. In actual practice, a particular combination of the above two types (wave cutting and wave removing) is the case. Therefore, the static rake angle is modified by the incremental variation of angle. This incremental variation can be represented as:

$$\mathrm{d}\psi = \mathrm{d}\psi_1 + \mathrm{d}\psi_2 \quad (24)$$

Bearing in mind the foregoing consideration, one may express Eq. (23) as follows:

$$\mathrm{d}\psi = s_1 \mathrm{d}\zeta + s_2 \mathrm{d}\alpha + s_2 \mathrm{d}\psi \quad (25)$$

where s_1 and s_2 are:

$$s_1 = \frac{-\cos\alpha}{(\zeta - \sin\alpha)^2 \left[1 + \left(\frac{\cos\alpha}{\zeta - \sin\alpha} \right)^2 \right]}$$
$$s_2 = \frac{1 - \zeta \sin\alpha}{(\zeta - \sin\alpha)^2 \left[1 + \left(\frac{\cos\alpha}{\zeta - \sin\alpha} \right)^2 \right]} \quad (26)$$

The compression ratio ζ can be written as [2]:

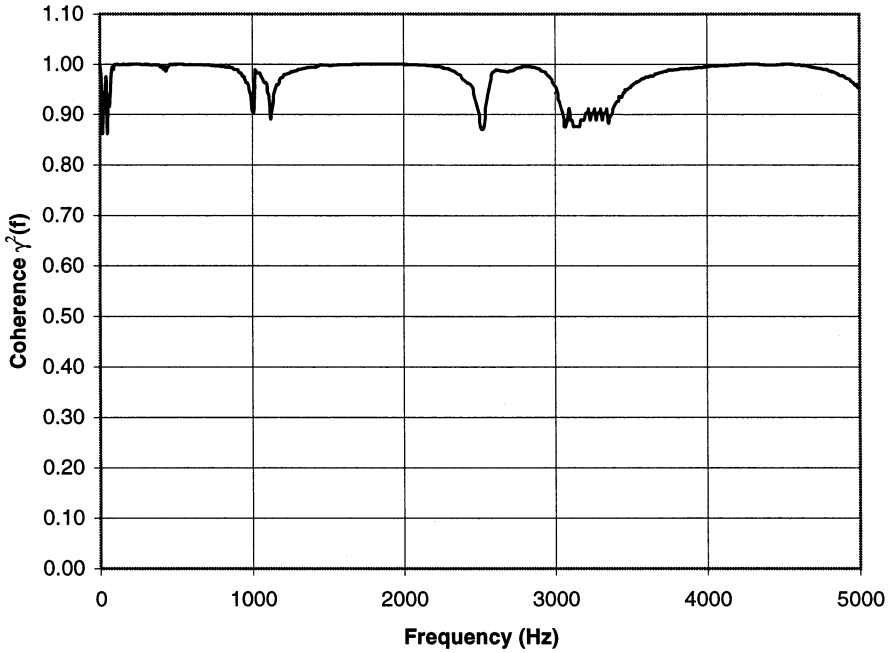

Fig. 7. Coherence of the dynamometer thrust signal vs. the hammer signal.

$$\zeta = \frac{1}{e\sin\alpha + (1 - f\sin\alpha)\left[g + \dfrac{h}{(4\times 10^4 t)^p}\ln\left(\dfrac{40t(200v)^n}{q}\right)\right]} \tag{27}$$

where e, f, g, h, p, n and q are constants, t is the undeformed chip thickness (m) and v is the cutting speed (m s^{-1}).

As might be expected, the chip compression ratio varies with other cutting parameters [19,20]. The incremental variation of the compression ratio ζ can be represented by its total differential in the following form:

$$d\zeta = \frac{\partial\zeta}{\partial t}dt + \frac{\partial\zeta}{\partial v}dv + \frac{\partial\zeta}{\partial\alpha}d\alpha \tag{28}$$

which can be simplified as:

$$d\zeta = l_1\,dt + l_2\,dv + l_3 d\alpha \tag{29}$$

where l_1, l_2 and l_3 are:

$$l_1 = \frac{-(1 - f\sin\alpha)\left[\dfrac{h}{t(4\times 10^4 t)^k} + \dfrac{-kh}{(4\times 10^4 t)^{k+1}}\ln\left(\dfrac{40t(200v)^n}{q}\right)\right]}{\left[e\sin + 1 - f\sin\alpha)\left[g + \dfrac{h}{(4\times 10^4 t)^k}\ln\left(\dfrac{40t(200v)^n}{q}\right)\right]\right]^2}$$

$$l_2 = \frac{-(1 - f\sin\alpha)\left[\dfrac{h}{(4\times 10^4 t)^k}\left(\dfrac{n}{v}\right)\right]}{\left[e\sin\alpha + (1 - f\sin\alpha)\left[g + \dfrac{h}{(4\times 10^4 t)^k}\ln\left(\dfrac{40t(200v)^n}{q}\right)\right]\right]^2}$$

$$l_3 = \frac{-\left[e\cos\alpha + (1 - f\cos\alpha)\left[g + \dfrac{h}{4\times 10^4 t)^k}\ln\left(\dfrac{40t(200v)^n}{q}\right)\right]\right]}{\left[e\sin\alpha + (1 - f\sin\alpha)\left[g + \dfrac{h}{4\times 10^4 t)^k}\ln\left(\dfrac{40t(200v)^n}{q}\right)\right]\right]^2} \tag{30}$$

Substituting Eq. (29) into Eq. (25), one may obtain:

$$d\phi = s_1 l_1\,dt + s_1 l_2\,dv + (s_1 l_3 + s_2)\,d\alpha + s_2\,d\psi \tag{31}$$

The incremental variation of the shearing force is obtained by substituting Eqs. (29) and (31) into Eq. (20)

$$dF_f = P_1\,dt + P_2\,dv + P_3\,d\alpha + P_4\,d\psi \tag{32}$$

where P_1, P_2, P_3 and P_4 are:

$$P_1 = m_1 + m_2 l_1 + m_4 s_1 l_1$$

$$P_2 = m_2 l_2 + m_3 + m_4 s_1 l_2$$

$$P_3 = m_4 s_1 l_3 + m_4 s_2 + m_2 l_3 + m_5$$

$$P_4 = m_4 s_2 \tag{33}$$

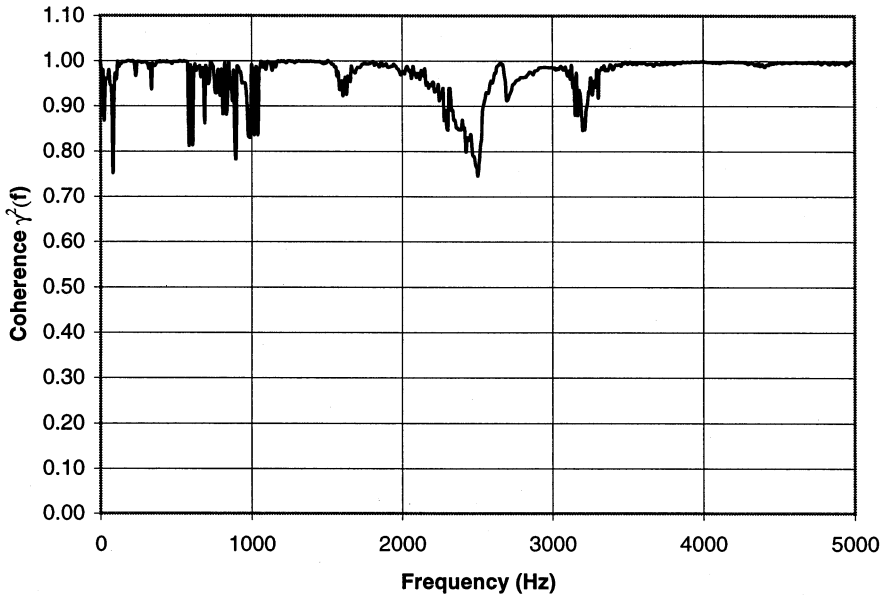

Fig. 8. Coherence of the dynamometer torque signal vs. the hammer signal.

Similarly, substituting Eq. (31) into Eq. (12), one may get

$$dF_s = T_1\,dt + T_2\,dv + T_3\,d\alpha + T_4\,d\psi \tag{34}$$

where T_1, T_2, T_3 and T_4 are:

$$T_1 = n_1 + n_2 s_1 l_1$$

$$T_2 = n_2 s_1 l_2$$

$$T_3 = n_2 s_1 l_3 + n_2 s_2 + n_3$$

$$T_4 = n_2 s_2 \tag{35}$$

Finally, the incremental variations of the cutting force's coordinate components are obtained by substituting Eqs. (31), (32) and (34) into Eq. (4):

$$dF_y = A_{ty}\,dt + A_{vy}\,dv + A_{\alpha y}\,d\alpha + A_{\psi y}\,d\psi \tag{36}$$

where A_{ty}, A_{vy}, $A_{\alpha y}$, $A_{\psi y}$ are:

$$A_{ty} = g_1 T_1 + g_2 P_1 + g_3 s_1 l_1$$

$$A_{vy} = g_1 T_2 + g_2 P_2 + g_3 s_1 l_2$$

$$A_{\alpha y} = g_1 T_3 + g_2 P_3 + g_3 s_1 l_3 + g_3 s_2 + g_4$$

$$A_{\psi y} = g_1 T_4 + g_2 P_4 + g_3 s_2 \tag{37}$$

and:

$$dF_x = A_{tx}\,dt + A_{vx}\,dv + A_{\alpha x}\,d\alpha + A_{\psi x}\,d\psi \tag{38}$$

where A_{tx}, A_{vx}, $A_{\alpha x}$, $A_{\psi x}$ are:

$$A_{tx} = e_1 T_1 + e_2 P_1 + e_3 s_1 l_1$$

$$A_{vx} = e_1 T_2 + e_2 P_2 + e_3 s_1 l_2$$

$$A_{\alpha x} = e_1 T_3 + e_2 P_3 + e_3 s_1 l_3 + e_3 s_2 + e_4$$

$$A_{\psi x} = e_1 T_4 + e_2 P_4 + e_3 s_2 \tag{39}$$

2.4. Interpretation of the incremental variations in terms of cutting process parameters

If the motion of the lower chip boundary is designated by $\dot{x}_1$, and the motion of the upper chip boundary is designated by $\dot{x}_2$, then the variations of the cutting parameters are given by:

$$d\alpha = \frac{\dot{x}_1}{v} \tag{40}$$

$$d\psi = \frac{\dot{x}_1 - \dot{x}_2}{v} \tag{41}$$

$$dv = \frac{\dot{x}_1^2}{2v} \tag{42}$$

and:

$$dt = x_1 - x_2 + \epsilon\,\frac{\dot{x}_1}{v} \tag{43}$$

where ϵ is the geometric lead of the free end of the shear zone relatively to its end on the tool cutting edge. Simple analysis of the model in Fig. 1 shows that:

$$\epsilon = t\cot\phi \tag{44}$$

Then Eq. (43) can be re-written as:

$$dt = x_1 - x_2 + t\cot\phi\,\frac{\dot{x}_1}{v} \tag{45}$$

Substituting Eqs. (40)–(42) and (45) into Eqs. (36) and (38), one may obtain:

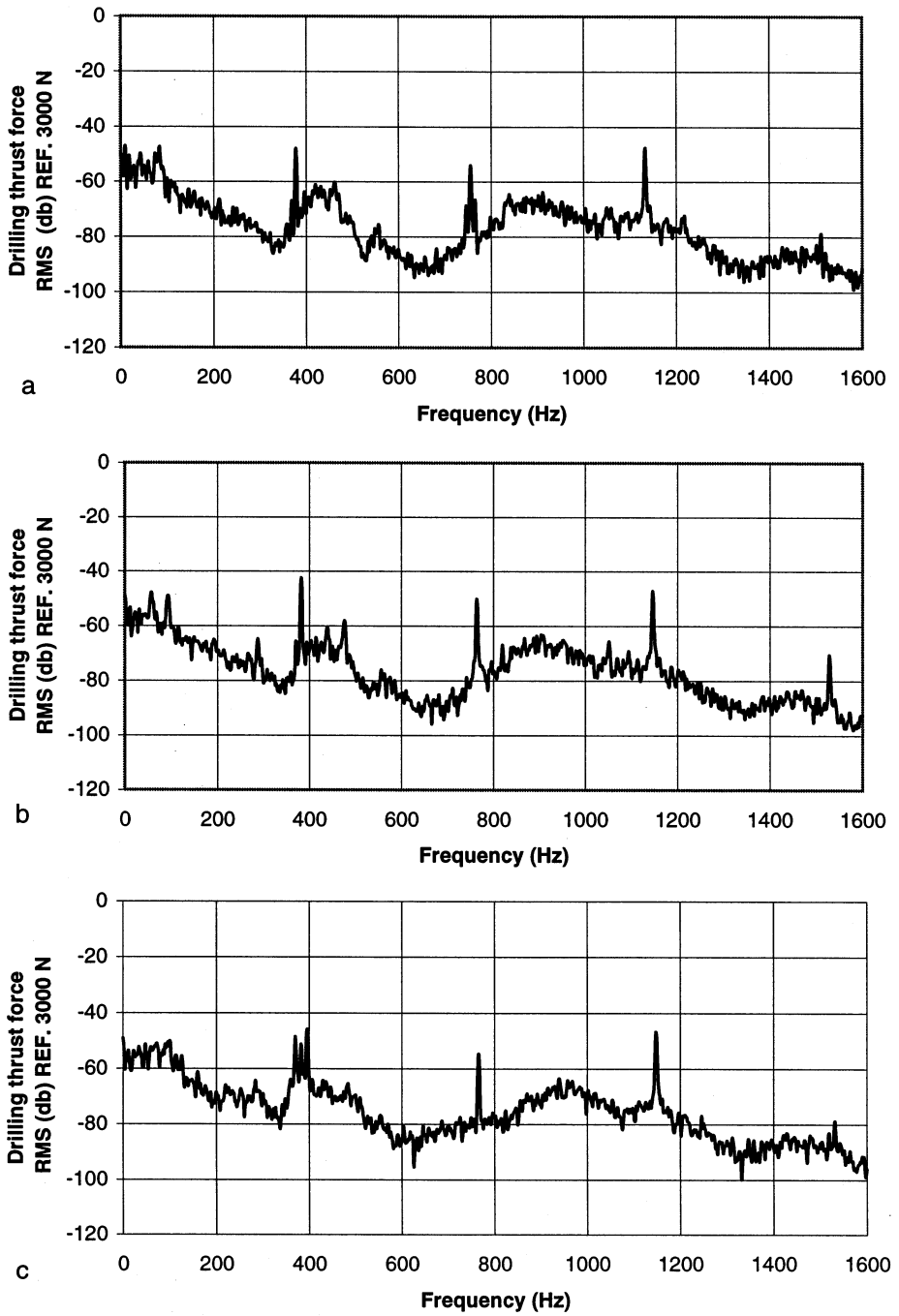

Fig. 9. Autospectra of the thrust force: (a) $n = 900$ rpm, $t = 0.125$ mm rev^{-1}; (b) $n = 1200$ rpm, $t = 0.125$ mm rev^{-1}; (c) $n = 1200$ rpm, $t = 0.1458$ mm rev^{-1}.

$$dF_y = A_{ty}\left(x_1 - x_2 + t\cot\phi\,\frac{\dot{x}_1}{v}\right) + A_{vy}\left(\frac{\dot{x}_1^2}{2v}\right) + A_{\alpha y}\left(\frac{\dot{x}_1}{v}\right) + A_{\psi y}\left(\frac{\dot{x}_1 - \dot{x}_2}{v}\right) \quad (46)$$

$$dF_x = A_{tx}\left(x_1 - x_2 + t\cot\phi\,\frac{\dot{x}_1}{v}\right) + A_{vx}\left(\frac{\dot{x}_1^2}{2v}\right) + A_{\alpha x}\left(\frac{\dot{x}_1}{v}\right) + A_{\psi x}\left(\frac{\dot{x}_1 - \dot{x}_2}{v}\right) \quad (47)$$

2.5. Equations of motion

Multiple observations and measurements of the profile of the surface of cut show that x_1 and x_2 may be assumed to be harmonic functions having corresponding frequencies ω_1 and ω_2, i.e.:

$$x_1 = X_1 \cos \omega_1 T$$

$$x_2 = X_2 \cos \omega_2 T$$

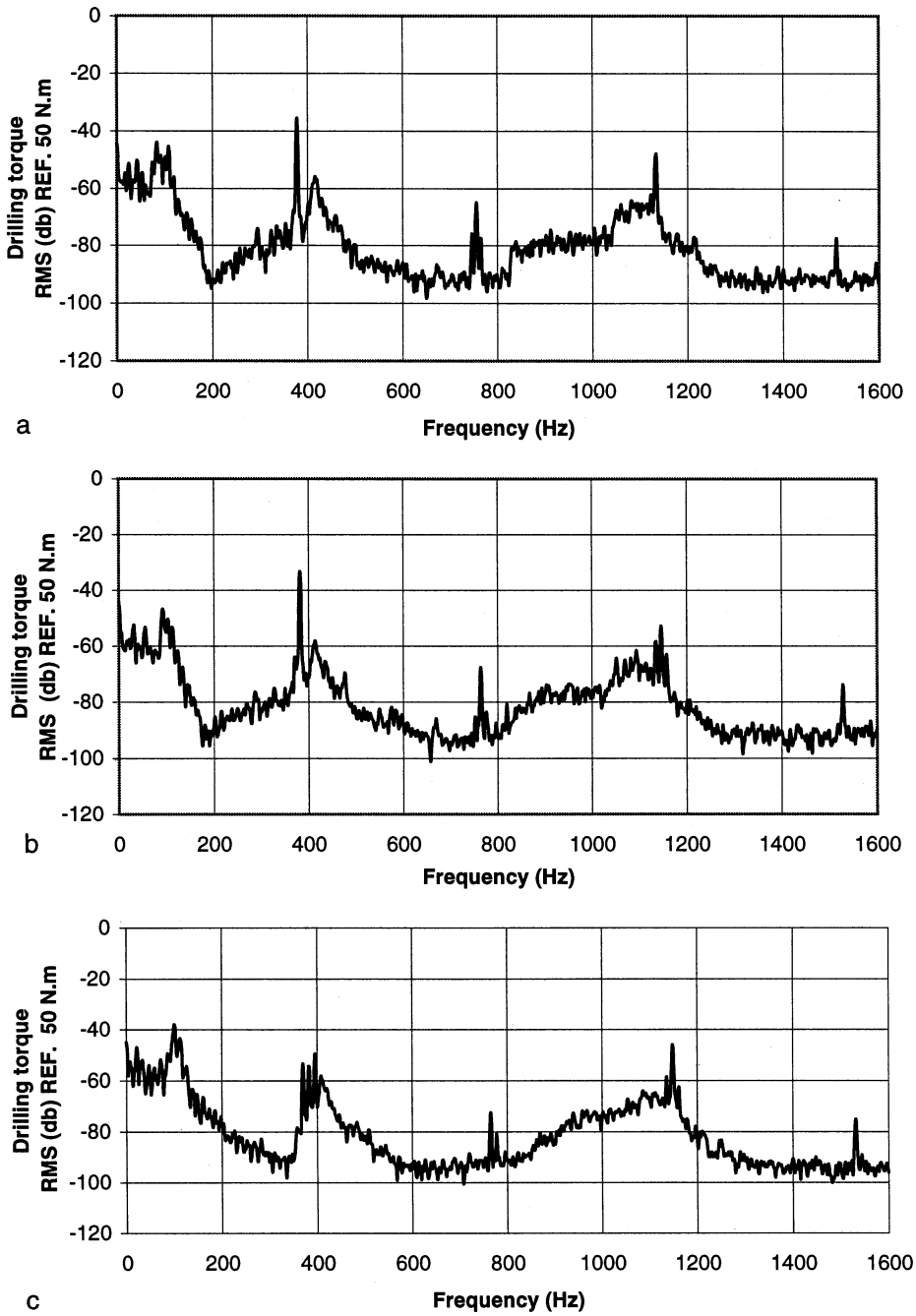

Fig. 10. Autospectra of the torque: (a) $n = 900$ rpm, $t = 0.125$ mm rev^{-1}; (b) $n = 1200$ rpm, $t = 0.125$ mm rev^{-1}; (c) $n = 1200$ rpm, $t = 0.1458$ mm rev^{-1}.

$$\dot{x}_1 = -X_1\omega_1 \sin \omega_1 T$$

$$\dot{x}_2 = X_2\omega_2 \sin \omega_2 T \quad (48)$$

Here ω_1, ω_2 are defined by the chosen cutting regime and the diameter of the workpiece if the chip formation process is stable [21].

2.6. Proposed model for the cutting forces evaluation

The proposed model for the cutting force evaluation is obtained by substituting Eq. (48) into Eqs. (46) and (47) and by substituting the result into Eq. (3):

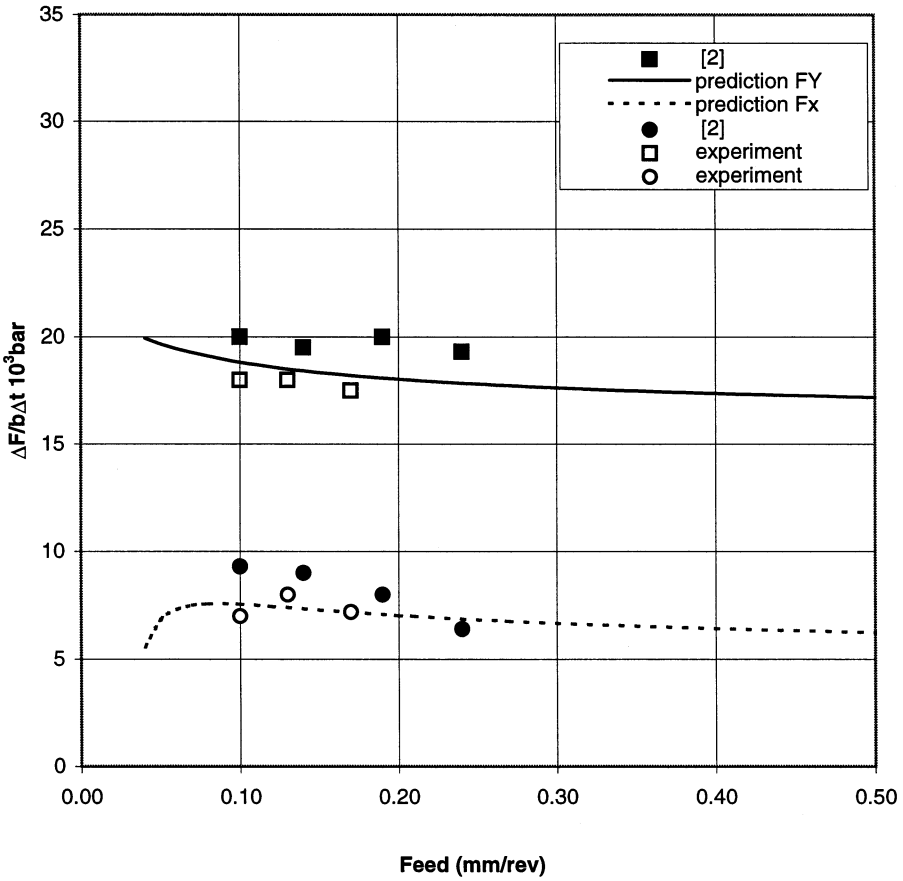

Fig. 11. Effect of the feed on the dynamic forces.

$$F_{yi} = F_y + \mathrm{d}F_y$$
$$= F_y + A_{ty}\left(X_1 \cos \omega_1 T - X_2 \cos \omega_2 T - t \cot \phi \frac{X_1 \omega_1 \sin \omega_1 T}{v}\right) + A_{vy}\left(\frac{X_1^2 \omega_1^2 \sin^2 \omega_1 T}{2v}\right) + A_{\alpha y}\left(\frac{-X_1 \omega_1 \sin \omega_1 T}{v}\right) + A_{\psi y}\left(\frac{-X_1 \omega_1 \sin \omega_1 T + X_2 \omega_2 \sin \omega_2 T}{v}\right) \quad (49)$$

and:

$$F_{xi} = F_x + \mathrm{d}F_x$$
$$= F_x + A_{tx}\left(X_1 \cos \omega_1 T - X_2 \cos \omega_2 T - t \cot \phi \frac{X_1 \omega_1 \sin \omega_1 T}{v}\right) + A_{vx}\left(\frac{X_1^2 \omega_2^1 \sin^2 \omega_1 T}{2v}\right) + A_{\alpha x}\left(\frac{-X_1 \omega_1 \sin \omega_1 T}{v}\right) + A_{\psi x}\left(\frac{-X_1 \omega_1 \sin \omega_1 T + X_2 \omega_2 \sin \omega_2 T}{v}\right) \quad (50)$$

2.7. Computer simulations

Four series of testing programs were carried out to assess the effects of the cutting feed, cutting speed, rake angle and frequency of the waves on the work surface on the dynamic force components F_x and F_y. Table 1 presents the cutting conditions and Table 2 presents the cutting regimes used in the simulations. Figs. 2–5 show the results of the simulation. As seen, the variations of the force components follow approximately sinusoidal waves. A certain phase lag relative to the variation of the uncut chip thickness is seen clearly.

3. Experimental verification of the proposed model

In order to assess the accuracy of the proposed model, a series of experiments was carried out. Since the dynamic parameters of orthogonal cutting are known to be very sensitive to even the smallest changes in the cutting process, special attention was paid to the selecting and verifying of the conditions of the tests and to the experimental methodology [13,22,23]. The test conditions were selected as follows:

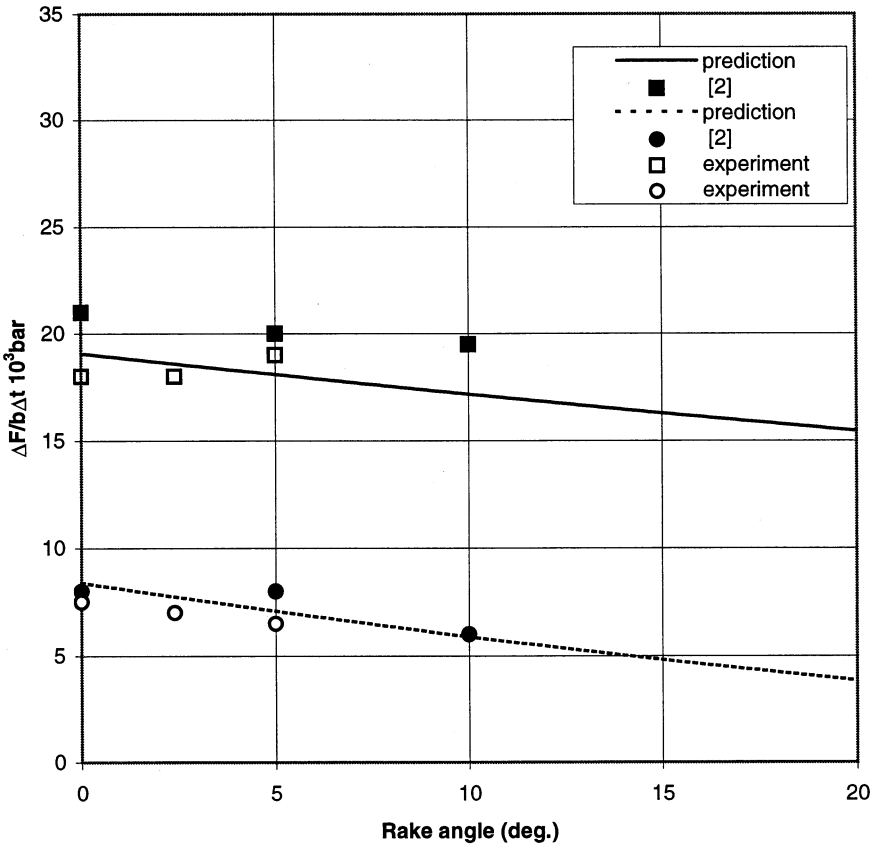

Fig. 12. Effect of the rake angle on the dynamic forces.

(1) Workpiece material: hot finished mild steel (AISI 1025, $\sigma_{ult} = 400$ MPa, $c_v = 4.0 \times 10^6$ J (K m^{-3}), $w = 8.00 \times 10^{-6}$ m^2 s^{-1}). The outer surface of the workpices has been waved using a CNC machine to obtain a sinusoidal wave with 0.05 mm amplitude. The composition, the element limits and the deoxidation practice had been chosen according to the requirements of standard ANSI/ASME B94.55M-1985 and were requested of the steel dealer. The hardness of the work material was 131 HB, being determined over the complete cross section of the terminal end of a tubular workpiece. Cutting tests were conducted only on the bars where the hardness was within the limits $\pm$ 10%. Special parameters such as the chemical composition, element counts, the microstructure, grain size, inclusions count, etc. were inspected using quantitative metallography.

(2) Machine: A retrofitted Schaerer HPD 631 boring machine was used. The drive unit motor was replaced with 15 kW variable speed AC motor and the feed motor was replaced with 5 kW variable speed AC motor. The motors are individually controlled by AC invertors, the latter being designed to provide the required volts–hertz ratio, allowing the AC motors to run at their optimum efficiency and providing the rated torque capability through the motor's rated base speed. The control section of the AC inventors consists of a control board with a 16-bit microprocessor and keypad interface with an 8-bit microprocessor.

(3) Cutting tool: A special tool holder [13] and indexable carbide inserts were used. The inserts were ground to different rake angles. The tool material was carbide C-6. The inserts used in the experiments were ground with a zero nominal cutting edge radius, the grinding being controlled using a computer-controlled optical corporator (Mitutoy PH 350). The actual radiuses did not exceed the value of 0.015 mm.

(4) Dynamometer: A 2-component piezo-electric load washer (Model 9065) has been used to measure the cutting forces. The tangential component of the cutting force F_y was estimated through the cutting torque whilst its radial component F_x was measured directly as the thrust force. The transducer incorporates two disks, each with a ring of quartz crystals oriented precisely in circumferential and axial directions. The load washer has been integrated into a dynamometer to be held in the chuck. Based on the standard mounting as specified by the supplier (Kistler), the load washer has been pre-loaded by two flanges to 120 kN. At this pre-load, the range for force measurements is from -20 to $+20$ kN the range for torque is from -200 to $+200$ N m. The dynamometer design has been presented in details earlier [24].

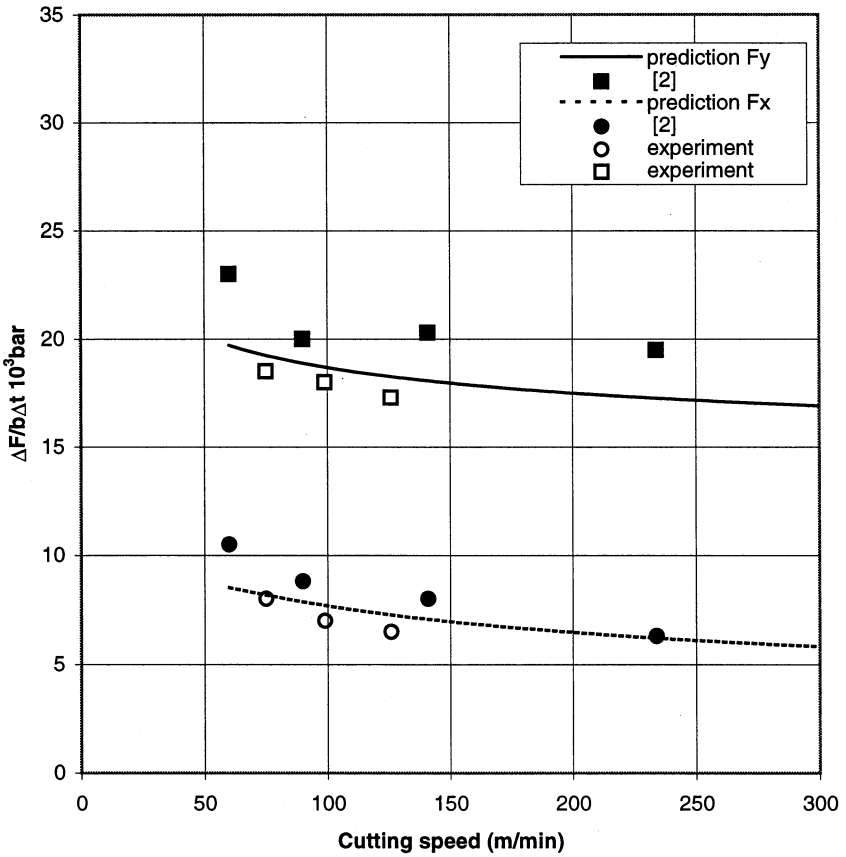

Fig. 13. Effect of the cutting speed on the dynamic forces.

(5) Measuring set-up: The load washer was connected to the charge amplifiers (Kistler model 5004) which, in turn, were connected to the dual-channel FFT spectrum analyser (B and K Analyzer Type 2032). The details of the static calibration were presented in detail earlier [24]. Also, the frequency response measurements of the set-up were carried out to determine the range of frequencies of the cutting forces that could be measured accurately without distortion. The load washer with allied charge pre-amplifiers and the FFT analyzer was calibrated by hammering the dynamometer with a Kistler hammer (Model 912), Fig. 6 showing the frequency response function vs. the hammer signal. The magnitude of the ratio of the output of the dynamometer to the force applied by the hammer was determined in the frequency range 0–1.6 kHz. Referring to Fig. 6, it can be inferred that cutting forces of up to 650 Hz can be measured without any distortion due to resonance influences. To examine the validity of the measurement, the coherence function has been calculated for the thrust force and the torque [25]. Figs. 7 and 8 show the coherence of the dynamometer thrust and torque force signals versus the hammering signals. As seen, the values of the experimentally-determined coherence functions are quite close to unity, assuring the measurement accuracy.

Analysis of the frequency composition was carried out to determine the variations in the coordinate components of the cutting force. Figs. 9 and 10 show autospectras for the thrust and torque, respectively. In the experiments, it was found that the frequencies of the character peaks in such autospectras are invariant of the chosen cutting regime. By this is meant that the dynamic rigidity of the set-up was sufficient, thus did not affect the results of the study. Moreover, it means that the force components are not of random nature, as considered in the earlier study [24,26,27].

Figs. 11–14 show the comparison between the predicted and the measured dynamic forces. Here, the experimental results obtained in [2] are shown also. The comparison shows that the proposed model gives good agreement with the experimental results.

4. Conclusions

A new model for analytical evaluations of the cutting forces in orthogonal cutting is proposed. The model utilizes the known advantages of the model of a shear zone with parallel boundaries proposed by Astakhov and Osman [13] for steady-state orthogonal cutting.

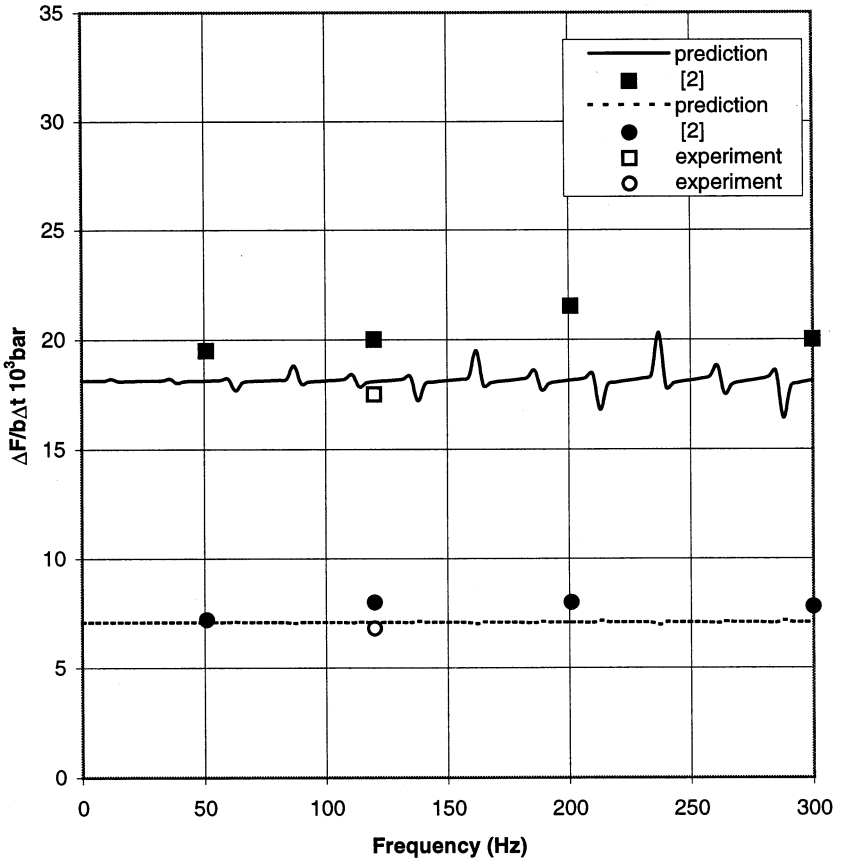

Fig. 14. Effect of the frequency on the dynamic forces.

This study shows that a shear zone with parallel boundaries responds to the dynamic variations in the cutting conditions. These variations follow approximately sinusoidal waves, the phases of which lag behind the uncut chip thickness.

The analysis of the frequency composition of the coordinate components of the cutting force shows that the frequencies of the character peaks in such autospectras are invariant of the chosen cutting regime. This establishes that the dynamic rigidity of the set-up was sufficient, and thus did not affect the results of the study.

In general, this investigation added a further verification to the theoretical model presented in [13]. The good correlation found between the experimental and the predicted dynamic cutting forces shows that the basic relationship of the cutting mechanics can be applied in the study of cutting dynamics.

5. Nomenclature

A_{ty}, A_{vy}, $A_{\alpha y}$, $A_{\psi y}$	coefficients in Eq. (36)
A_{tx}, A_{vx}, $A_{\alpha x}$, $A_{\psi x}$	coefficients in Eq. (38)
b	width of cut
c_v	specific heat capacity at constant volume
C_1, C_2, C_3, C_4	constants in Eq. (18)
e_1, e_2, e_3, e_4	coefficients in Eq. (4)
F_y, F_{yi}	mean tangential force and dynamic tangential force
F_x, F_{xi}	mean cutting force and dynamic cutting force
F_s, F_{si}	mean shear force and dynamic shear force
F_f, F_{fi}	mean friction force and dynamic friction force
g_1, g_2, g_3, g_4	coefficients in Eq. (4)
k	shear stress in the primary deformation zone
k_1	shear stress in the tool–chip interface zone
l_1, l_2, l_3	coefficients in Eq. (29)
l_{ef}	effective length the tool–chip interface
m_1, m_2, m_3, m_4	coefficients in Eq. (20)
n_1, n_2, n_3	coefficients in Eq. (12)
P_1, P_2, P_3 P_4	coefficients in Eq. (32)
s_1, s_2	coefficients in Eq. (25)

t, t_i	nominal uncut chip thickness and dynamic uncut chip thickness
T_1, T_2, T_3, T_4	coefficients in Eq. (34)
T_s	temperature in the primary deformation zone
T_f	temperature in the tool–chip interface zone
v, v_i	nominal cutting speed and dynamic cutting speed
x_1, $\dot{x}_1$	displacement of the tool tip and oscillation velocity of the tool tip
x_2, $\dot{x}_2$	displacement at the surface end of the shear zone and oscillation velocity at the surface end of the shear plane

Greek letters

α, α_i	nominal rake angle of the tool and dynamic rake angle of the tool
γ	strain in the shear zone
ζ, ζ_i	mean compression ratio and dynamic compression ratio
σ_{ult}	ultimate tensile strength of the workpiece
ϕ, ϕ_i	mean shear angle and dynamic shear angle
ψ	angle between the free surface of the workpiece and the y-direction
ω_1	frequency of the tool variation
ω_2	frequency of the work surface slope variation

Acknowledgements

The financial support of the Natural Science and Engineering Research Council of Canada and the Canadian International Development Agency is gratefully acknowledged.

References

[1] E.J. Armarego, The Mechanics of Metals, Prentice-Hall, 1969.
[2] M.M. Nigm, M.M. Sadek, S.A. Tobias, Determination of dynamic cutting coefficients from steady state cutting data, Int. J. Mach. Tool Des. Res. 17 (1977) 19–37.
[3] J. Peters, P. Vanherck, H. Van Brussel, The measurement of the dynamic cutting force coefficients, CIRP Annals. 21 (2) (1971) 129–136.
[4] J. Tlusty, B.S. Goel, Measurement of the dynamic cutting force coefficient, in: Proceedings of the Second NAMRI Conference, 1974, Madison, WI, pp. 649–659.
[5] J. Tlusty, O. Heczko, Improving tests of damping in the cutting process, in: Proceedings of the Eighth NAMRI Conference, 1980, Rolla, MO, pp. 372–386.
[6] K. Das, S.A. Tobias, The relation between the static and the dynamic cutting of metals, Int. J. Mach. Tool Des. Res. 7 (1967) 63–75.
[7] C. Rubenstein, An analysis of dynamic cutting when a plane surface is cut with an oscillating tool—Part I: general equations, Int. J. Mach. Tool Des. Res. 12 (1972) 179–191.
[8] D.W. Wu, C.R. Liu, An analytical model of cutting dynamics—Part 1: model building, ASME J. Eng. Ind. 107 (1985) 107–111.
[9] D.W. Wu, C.R. Liu, An analytical model of cutting dynamics—Part 2: verification, ASME J. Eng. Ind. 197 (1985) 112–118.
[10] D.W. Wu, Governing equations of the shear angle oscillation in dynamic orthogonal cutting, ASME J. Eng. Ind. 108 (1986) 280–291.
[11] D.W. Wu, Comprehensive dynamic cutting force model and its application to wave-removing processes, ASME J. Eng. Ind. 110 (1988) 153–161.
[12] D.W. Wu, A new approach of formulating the transfer function for the dynamic cutting processes, ASME J. Eng. Ind. 111 (1989) 37–47.
[13] V.P. Astakhov, M.O.M. Osman, An analytical evaluation of the cutting forces in self-piloting drilling using the model of shear zone with parallel boundaries—Part 1: theory, Int. J. Mach. Tools Manuf. 36 (11) (1996) 1187–1200.
[14] P.L.B. Oxley, Mechanics of Machining—An Analytical Approach To Assessing Machinability, Ellis Horwood, Chichester, 1989.
[15] M.E. Merchant, Mechanics of the metal cutting process—Part I: orthogonal cutting and a type chip—Part II, plasticity conditions in orthogonal cutting, J. Appl. Phy. 16 (1945) 267–275 and 318–324.
[16] G. Dieter, Mechanical Metallurgy," 3rd ed., McGraw–Hill, New York, 1986.
[17] V.S. Kushner, Thermomechanical Approach in Metal Cutting, Irkutsk Univ. Pabl. Ltd, 1982 (In Russian).
[18] N.N. Zorev, Metal Cutting Mechanics, Pergamon Press, 1966.
[19] V.P. Astakhov, M.O.M. Osman, Correlations amongst process parameters in metal. cutting and their use for establishing the optimum cutting speed, J. Mat. Proc. Tech. 62 (1996) 175–179.
[20] M.M. Nigm, M.M. Sadek, Experimental investigation of the characteristics of dynamic cutting process, ASME J. Eng. Ind. 98 (1977) 410–418.
[21] V.P. Astakhov, S.V. Shvets, M.O.M. Osman, Chip structure classification based on mechanism of its formation, J. Mat. Proc. Tech. 71 (1997) 247–257.
[22] V.P. Astakhov, M. Al-Ata, M.O.M. Osman, Statistical design of experiments in metal cutting—Part 1: methodology, J. Test Evac. 25 (1997) 322–327.
[23] V.P. Astakhov, M. Al-Ata, M.O.M. Osman, Statistical design of experiments in metal cutting–Part 2: application, J. Test Evac. 25 (1997) 328–334.
[24] S. Chandrashekhar, M.O.M. Osman, T.S. Sankar, An experimental investigation for the stochastic modelling of the resultant force system in BTA deep-hole machining, Int. J. Prod. Res. 23 (4) (1985) 657–673.
[25] J.S. Bendat, A.G. Piersol, Random data: analysis and measurement procedures, Wiley-Interscience, New–York, 1971.
[26] M.O.M. Osman, T.S. Sankar, Short-time acceptance test for machine tools based on the random nature of the cutting forces, Trans. ASME J. Eng. Ind. 94 (1972) 1020–1024.
[27] T.S. Sankar, M.O.M. Osman, Profile characterization of manufactured surfaces using random function excursion technique—Part 1: theory, Trans. ASME J. Eng. Ind. 97 (1975) 190–195.